11.4 A Fast-Readout Mismatch-Insensitive Magnetoresistive Biosensor Front-End Achieving Sub-ppm Sensitivity

Xiahan Zhou, Michael Sveiven, Drew A. Hall

University of California, San Diego, La Jolla, CA

Magnetic biosensors have drawn significant research interest as a means to replace large optical instrumentation commonly found in centralized diagnostic laboratories. Magnetic biosensing is attractive since biological samples lack a magnetic background thus enabling high sensitivity measurements. Figure 11.4.1 shows a magnetic immunoassay where: 1) the surface of a magnetic sensor is coated with capture molecules (e.g., antibodies) specific to the biomarker (e.g., antigen) of interest, 2) the sample, detection molecules, and magnetic nanoparticles (MNPs) are added and self-assemble thus tethering the MNPs to the sensor, and 3) the sensor is read out by applying a magnetic field, H_A, that magnetizes the superparamagnetic MNPs producing a stray field that perturbs the local magnetic field. The underlying magnetoresistive (MR) sensor detects this change in field as a miniscule ppm change in resistance, R_{sig}, that is directly proportional to the number of MNPs. Unfortunately, R_{sig} is superimposed on the baseline resistance, R_0, resulting in a large baseline-to-signal ratio (R_0/R_{sig}>10,000) that requires a very high dynamic range (DR>120dB) front-end for quantitative detection [1,2].

Traditional techniques such as a Wheatstone bridge are limited by the sensor-to-sensor matching, which is often no better than 5 to 10%, even on the same die [3]. Other techniques such as magnetorelaxometry solve the baseline issue by self-referencing using a pulsed magnetic field but require high-speed digitization to capture the fast (<1μs), transient relaxation signal and need averaging to deal with the noise [2]. Magnetic double-modulation is another technique that separates the signals spectrally and reduces the 1/*f* noise from the sensors and AFE; but most implementations perform the down modulation and lock-in digitally thus still requiring high DR ADCs and only improve the baseline-to-signal ratio by an order of magnitude [3-5]. This paper presents a CMOS front-end for MR biosensors that can tolerate up to 10% sensor mismatch and achieves sub-ppm sensitivity with an input-referred noise PSD of 46.4nT/√Hz, input-referred baseline of <0.235mT, power consumption of 1.39mW, and readout time of 11ms owing to: 1) a double modulation bias scheme with reference sensors that reduces baseline/signal to <20 and a built-in down-modulator that relaxes the ADC bandwidth, 2) fast settling duty-cycled resistors (DCRs) that reduce the settling time by 40× compared to traditional DCRs, and 3) a high-frequency interference-rejection (HFIR) sampling technique that reduces out-of-band interference and thus the required ADC DR.

The chip architecture is shown in Fig. 11.4.2 where a sinusoidal bias current at frequency f_C is injected into a giant magnetoresistive (GMR) sensor array placed inside of an external Helmholtz coil that generates a sinusoidal magnetic field at frequency f_H. Output spectra shows that the signal of interest is modulated to $f_C \pm f_H$ while the R_0 baseline remains at f_C. A mux selects an active and a reference sensor that are fed to the programmable gain amplifier (PGA) which rejects the common-mode signal thus eliminating most of the baseline (>90%). The PGA also down-modulates the signal to DC relaxing the ADC bandwidth. However, the sensor mismatch (in both MR and R_0) causes baselines at DC and f_H that are still up to 20× and 800× larger than the signal of interest, respectively. Left unaddressed, these would still require a high DR ADC; instead, we propose a sampling scheme that reduces the interference before it is seen by the ADC.

The PGA is implemented by a capacitive feedback amplifier, where the gain C_1/C_2 is set by a 2b programmable capacitor (Fig. 11.4.3). Inputs V_S and V_{ref} contain large common-mode swing and the outputs also have large swing mainly due to the interference at f_H. The DC operating points were chosen to maximize both swings. Since the output swing is highly dependent on the sensor mismatch, the PGA can be programmed for high gain in low mismatch scenarios to improve the SNR. The OTA uses switched-capacitor common-mode feedback (SC-CMFB) to maximize the output swing and integrates choppers at the cascode node for down-modulation. This amplifier is designed for fast settling needed when multiplexing sensors. The sudden closing of the row select switches (Sel: 0→1) causes a large transient at V_{in}, which takes a long time to settle when using a traditional DCR or a pseudo-resistor for biasing since the bias resistors must be large for low noise. To address this, the switches controlled by φ_{dcr} remain closed during and after sensor selection for 0.1ms, thus providing a low impedance path from V_{in} to V_{cmi} enabling fast settling. The fast settling DCRs reduce the settling time by 40×.

The ADC is implemented by a 1st-order incremental ΔΣ modulator (Fig. 11.4.4) with an oversampling ratio of 10,000. As shown in Fig. 11.4.2, the interference at the ADC input can be as large as 200mV, while the MR baseline and signal at DC are <10mV. While out-of-band, this interference eats into the DR and cannot be easily low-pass filtered without enduring a prohibitively long settling time. Instead, we propose a feed-forward high-pass filtering technique in the sampling network. A high-pass filtered version of the signal is first sampled onto the bottom plate of C_4. Subsequently, the signal is sampled onto the top plate of C_4, thus cancelling the high frequency interference. The HFIR is implemented by a pseudo-differential switched-capacitor high-pass filter followed by a chopped buffer to reduce offset and 1/*f* noise. A modified correlated double sampling (CDS) technique is applied to remove the OTA offset and 1/*f* noise. Specifically, switches $S_{1,2}$ were added to isolate C_6 from V_{ac} so that C_6 only samples the offset from the OTA during the sampling phase. A 16b counter and a shift register decimate the bitstream and serialize the output, respectively.

The chip in 180nm CMOS consumes 1.39mW excluding the sensor bias (ADC: 69%, PGA: 19%, digital blocks and bias: 12%). Figure 11.4.5 shows electrical measurement results where the PGA settling time is 50μs with the proposed DCR compared to a traditional DCR and pseudo-resistor which take 2ms and >14ms, respectively. The ADC DR for various sensor mismatches is shown where this design achieves significant improvements (>74dB for >2% mismatch) due to the HFIR technique that otherwise saturates the ADC. The ADC has an ENOB of 12.1b in the 100Hz bandwidth and provides 16dB interference suppression at f_H=10kHz. The fast readout time can be traded off for sensitivity, where this design achieves 0.98ppm sensitivity (147μΩ), which corresponds to ~2200 MNPs (d=50nm) with a SNR of 6dB.

The chip was connected to GMR sensor arrays to demonstrate the magnetic immunoassay. One sensor array was functionalized with biotinylated-bovine serum albumin (Biotin-BSA) and the other human Interleukin 6 (IL-6), a cancer biomarker. Both chips had BSA negative controls to monitor nonspecific binding and the reference sensor was covered by epoxy. Figure 11.4.6 shows measured real-time binding curves clearly differentiating the active and control sensors. The chip performance is summarized and compared to state-of-the-art solutions. Compared with other magnetometry-based designs, this work achieves 22.7× faster readout time, >7.8× lower baseline, and 2.3× lower power (see Fig. 11.4.6). Although relaxometry-based designs inherently eliminate the baseline, their lower signal amplitude and higher input-referred noise preclude high-sensitivity measurements [2]. This chip can tolerate up to 10% sensor mismatch, making it compatible with commercial tolerances for MR sensor fabrication. The sub-ppm sensitivity, low power consumption, and fast readout make this work ideal for multichannel, high sensitivity, point-of-care diagnostics. Figure 11.4.7 shows a die photo.

Acknowledgements:
This work was supported in part by Qualcomm, Inc. and the National Science Foundation (grant ECCS-1454608). The authors would like to thank MagArray, Inc. for providing the GMR sensors.

References:
[1] H. Wang, et al., "A Frequency-Shift CMOS Magnetic Biosensor Array with Single-Bead Sensitivity and no External Magnet," *ISSCC Dig. Tech. Papers,* pp. 438-439, Feb. 2009.
[2] S. Gambini, et al., "A 10 kPixel CMOS Hall Sensor Array with Baseline Suppression and Parallel Readout for Immunoassays," *IEEE JSSC,* vol. 48, no. 1, pp. 302-317, 2013.
[3] T. Costa, et al., "A CMOS Front-End with Integrated Magnetoresistive Sensors for Biomolecular Recognition Detection Applications," *IEEE TBioCAS,* vol. 11, no. 5, pp. 988-1000, 2017.
[4] S.J. Han, et al., "A High-Density Magnetoresistive Biosensor Array with Drift-Compensation Mechanism," *ISSCC Dig. Tech. Papers,* pp. 168-169,594, Feb. 2007.
[5] D.A. Hall, et al., "A 256 Pixel Magnetoresistive Biosensor Microarray in 0.18 um CMOS," *IEEE JSSC,* vol. 48, no. 5, pp. 1290-1301, 2013.

 978-1-5386-8531-0/19/$31.00 ©2019 IEEE

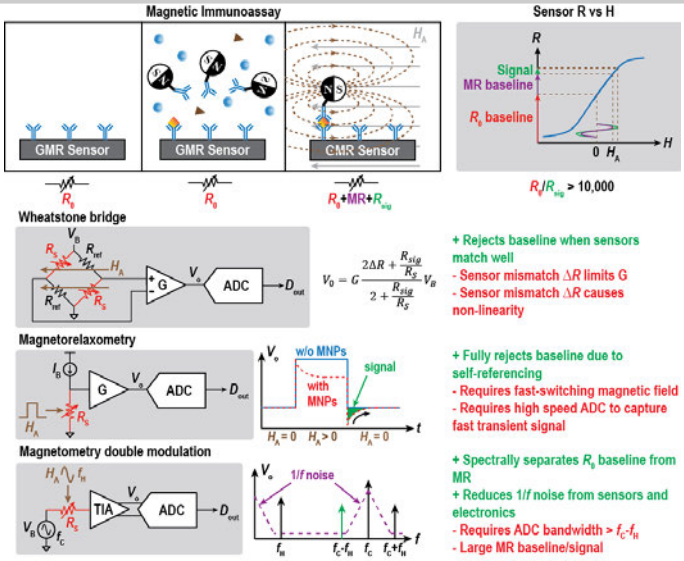

Figure 11.4.1: Magnetic immunoassay and prior readout architectures.

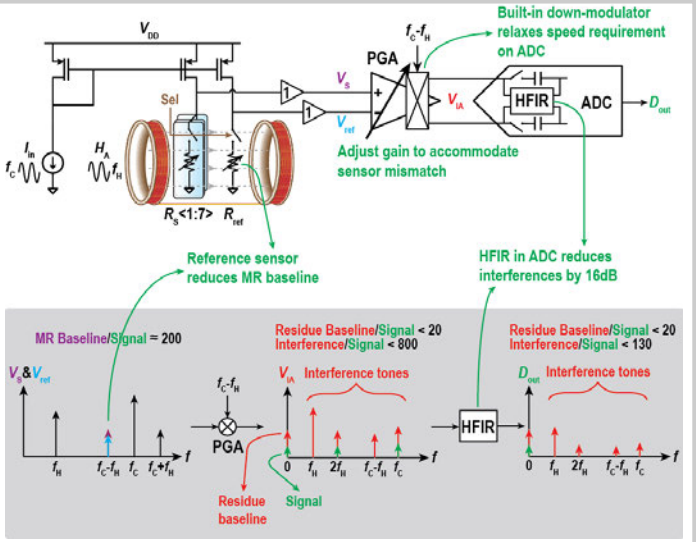

Figure 11.4.2: Architecture of the analog front-end and baseline/interference rejection diagram.

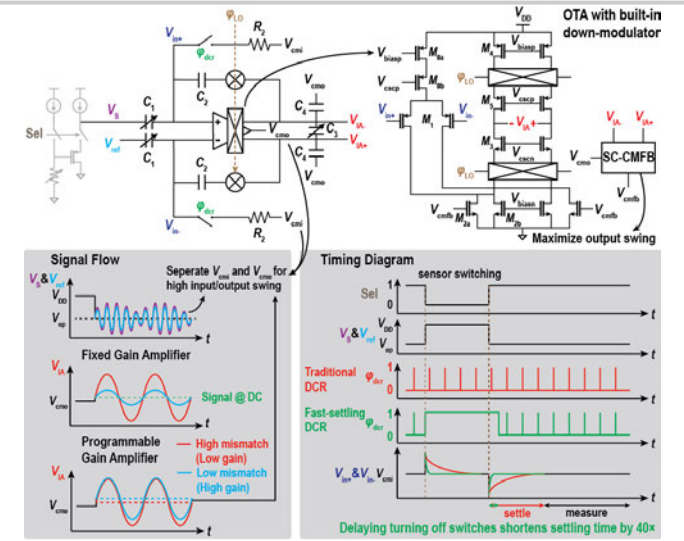

Figure 11.4.3: Schematic of the programmable gain amplifier and timing diagram.

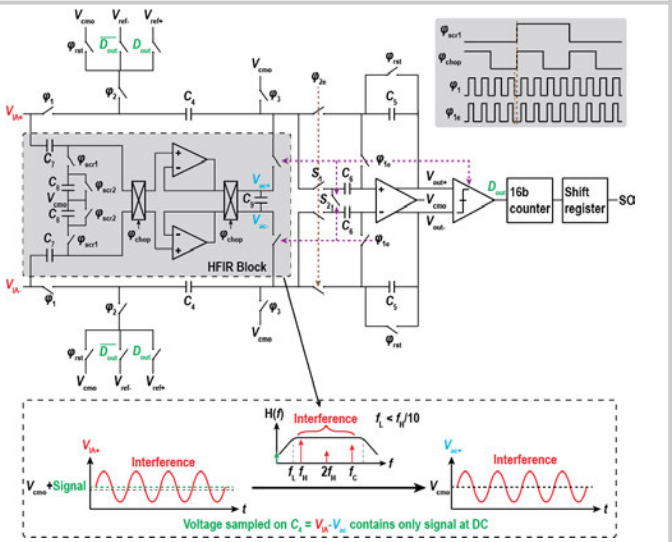

Figure 11.4.4: Schematic of the incremental ΔΣ ADC with high-frequency interference-rejection sampling.

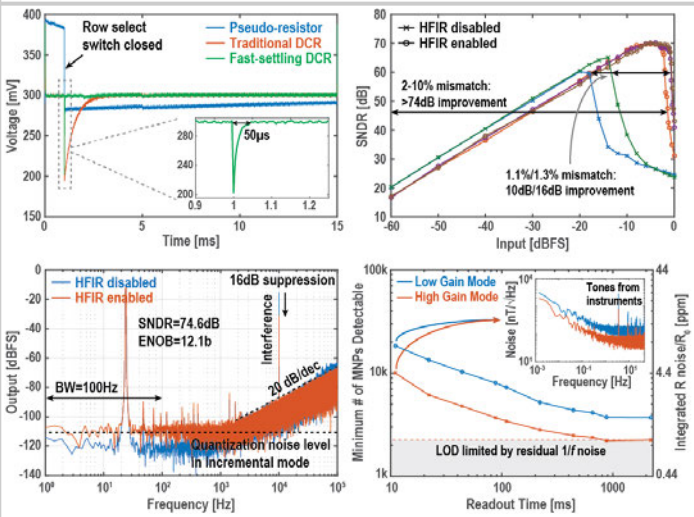

Figure 11.4.5: Measured PGA settling transient (top left), ADC dynamic range (top right), ADC output spectrum (bottom left), and system sensitivity (bottom right).

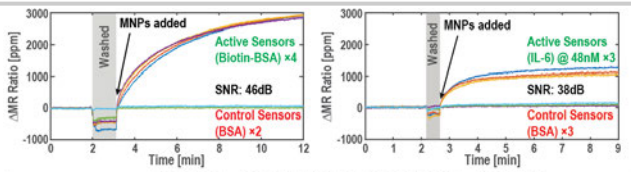

	ISSCC 2009 [1]	JSSC 2013 [2]	TBioCAS 2017 [3]	ISSCC 2007 [4]	JSSC 2013 [5]	This Work
Sensor Type	LC	Hall	GMR	GMR	GMR	GMR
Sensor Resistance (kΩ)	N/A	N/A	0.85	N/A	1.92	0.15
MR Ratio (%)	N/A	N/A	5.37	N/A	9.2	9.04
MNP Size (nm)	1,000	1,000	250	50	50	50
Technology (µm)	0.13	0.18	0.35	0.25	0.18	0.18
AFE Architecture	LC oscillator	V/I converter	Amplifier	Mixer + PGA	TIA	PGA with Mixer
ADC Architecture	VCO-based	Inc. ΔΣ	No ADC	No ADC	ΔΣ	Inc. ΔΣ + HFIR
Input-referred Noise (nT/√Hz)	N/A	270	11.5ᵠ	N/A	49	107.1 (low gain) 46.4 (high gain)
Sensor Mismatch Tolerance	N/A	N/A	N/A	N/A	N/A	10% (low gain) 2.5% (high gain)
Power/Ch (mW)*	N/A	0.825	4.9ᵠ	N/A	3.15	1.39
Area/Ch (mm²)	N/A	0.012	3.17	N/A	0.219	0.249
Input-referred Baseline (mT)	N/A	0.007	1.84	N/A	7.09	< 0.235
Readout Time/Ch (ms)	400ᵗ	50	1,000	250	250	11

* Does not include sensor bias and magnetic field generator.
ᵠ Does not include power and noise from ADC.
ᵗ Read from figures.

Figure 11.4.6: Magnetic assay real-time measurements (top) and comparison table (bottom).

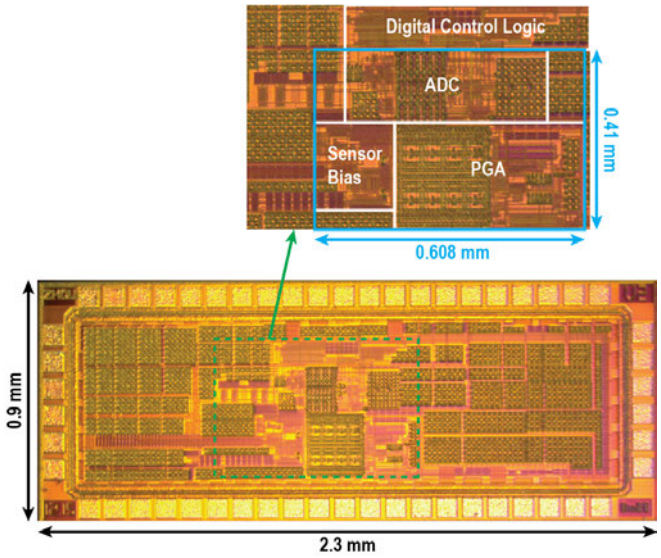

Figure 11.4.7: Die photo.

978-1-5386-8531-0/19/$31.00 ©2019 IEEE